Noble Gas MHD Generator Experiments At Low Stagnation Temperatures

Author(s): A. Veefkind, W. M. Hellebrekers, C. A. Borghi, and L. H. Th. Rietjens

Session Name: Closed Cycle

SEAM: 17 (1978)

SEAM EDX URL: https://edx.netl.doe.gov/dataset/seam-17

EDX Paper ID: 765

NOBLE GAS MHD GENERATOR EXPERIMENTS AT LOW STAGNATION TEMPERATURES

A.Veefkind, W.M.Hellebrekers, C.A.Borghi* and L.H.Th.Rietjens
Group Direct Energy Conversion
Eindhoven University of Technology,
Eindhoven, THE NETHERLANDS

Abstract

The performance of a noble gas MHD generator at stagnation temperatures of 2000 K and lower has been investigated experimentally in the MHD shock tunnel facility. The electrical power becomes equal to zero at stagnation temperatures around 1700 K. The decrease of the power is accompanied by a strong increase in the inlet relaxation length. The results, including the minimum stagnation temperature of 1700 K, are strongly dependent on the magnetic induction. At an inlet stagnation temperature of 2000 K a maximum enthalpy extraction of 11.5% was achieved. It follows from fast photography observations that at low stagnation temperatures the discharge is strongly inhomogeneous. The observed streamer velocity agrees with the calculated gas velocity in the core flow. Close to the electrode wall different streamer velocities are observed. The relative fluctuations measured in the electrode currents and the electron number density are larger at low stagnation temperatures than at high stagnation temperatures. The relative fluctuation level in the electron temperature did not change with the stagnation temperature. Cross correlation functions have been generated for the fluctuations of currents at different electrodes. At low as well as at high stagnation temperatures large correlation coefficients are found. Time shifts correspond to a velocity which agrees with the calculated gas velocity. The measured characteristics of the fluctuations are applied to different models of discharge structure.

I. Introduction

Nonequilibrium MHD generators will be operated at an inlet stagnation temperature of 2000 K. As the enthalpy extraction has to be above 20%, sufficient electrical conduction should be realized at stagnation temperatures below 1600 K near the exit. For supersonic generators this means that by nonequilibrium ionization an appreciable electrical conductivity has to be achieved at gas temperatures below 1000 K.

In order to obtain more information on the behaviour of noble gas MHD generators at the low temperature limit, this situation has been studied experimentally in the Eindhoven shock tunnel generator. Because the channel length (80 cm) is small and the maximum magnetic induction (3.3 T) low, it is not possible to achieve 20% enthalpy extraction at an inlet stagnation temperature of 2000 K. Therefore, the inlet stagnation temperature has been varied from about 2200 down to the value where the power production stops.

It has been observed earlier that the discharge structure in a nonequilibrium generator is inhomogeneous[1,2]. Because this inhomogeneity becomes very pronounced at low temperatures, the discharge is studied in more detail with an image converter streak camera. The purpose of this part of the work is to provide in a more extensive set of experimental data on discharge structures at different magnetic inductions and different stagnation temperatures.

As described in Ref.3 fluctuation analysis in MHD generators is a substantial part of our experimental program. The main topic now is to predict the electrode currents and electric power output using the measured electric fields and measured values of electron density and electron temperature including their fluctuations. To do this two models for the plasma inhomogeneities have been employed at stagnation temperatures around 2000 K. The first is the layer model including a streamer angle and the second is based on a model with isotropic inhomogenities.

II. Experimental arrangement

The MHD shock tunnel facility has been described earlier[4]. For the experiments described here a lexan channel was used with diverging insulator walls and parallel electrode walls. The length is 80 cm. The inlet cross section is 3.8 x 12 cm^2, the exit cross section 12 x 12 cm^2. Cylindrical stainless steel electrodes have been countersunk half way in the walls. Their diameter is 7 mm and their mutual distance 2.5 cm. The inlet Mach number of the channel is 1.6. A simple pre-ionization system was used by applying an external voltage from a battery of 290 V to the first two electrode pairs.

The working gas is cesium seeded argon. Recombination radiation, line reversal method, piezoelectric pressure transducers and electric probes are employed as diagnostics. The stagnation conditions, the measured pressures and the measured currents are used as an input in a gasdynamical program in which the one-dimensional stationary gasdynamic equations are solved to obtain the gas temperature, pressure and velocity as a function of the distance in the channel.

For the analysis of the fluctuations, signals are recorded on magnetic tape at high tape speed (240"/s) and played back at low tape speed (15/16"/s). The data handling has been described in Ref.3.

III. Generator performance

Current distributions along the generator at several stagnation temperatures are given in Fig.1. For all the runs presented the magnetic induction was around 3 T. Lower stagnation temperatures have been tried, but no power production was observed. From the gasdynamical program the stagnation temperature interval of each run has been calculated. The intervals are indicated in Fig.1 and plotted in Fig.2. It is assumed in

*Visiting scientist of the University of Bologna, Italy.

these calculations that the heat dissipated in the electrode boundary layer remains in the gas. If part of that heat is considered as a loss, then the exit stagnation temperatures are lower by an amount determined by the total current and the voltage drop. Roughly the maximum effect is an increase of the stagnation temperature interval by a factor 1.5 at a voltage drop of 50 V. It can be seen from Fig.2 that no stagnation temperatures below the level of 1700 K could be realized in a power producing working gas. The decrease of the electrical power with the inlet stagnation temperature is presented in Fig.3. In order to take into account small variations in the magnetic induction the power has been taken relative to the square of the magnetic induction. In this figure also those runs with an inlet stagnation temperature around 1700 K are included, where no power production has been measured. With a load resistance of 1.26 Ω as well as 2.26 Ω the power drops to zero between 1700 and 1800 K inlet stagnation temperature. With an inlet Mach number of 1.6 the gastemperature is then between 915 and 970 K.

In spite of the pre-ionization system a considerable increase of the relaxation length with decreasing stagnation temperature has been observed, in agreement with the results of Ref.5 which refer to experiments without pre-ionization. At stagnation temperatures around 2000 K the inlet relaxation length could be reduced by pre-ionization. At stagnation temperatures below 2000 K the pre-ionizer discharge could not be maintained by the plasma downstream. In Fig.4 the increase of the relaxation length and the decrease of the maximum current with decreasing inlet stagnation temperature has been visualized. The relaxation length is represented by the electrode number at which half the maximum current is achieved. Although both effects are significant, it seems that the growth of the relaxation length is a faster process than the reduction of the maximum current, when inlet stagnation temperatures become smaller.

A stagnation temperature of 1700 K should not be considered as an absolute low performance limit of the MHD conversion process. In the first place a low stagnation temperature at the inlet is not completely analogeous to a low stagnation temperature at the exit of a generator. Presumably of even more importance in the influence of the magnetic induction on the results. Fig.5 shows the current distribution along the generator at various values of the magnetic induction between 2.0 and 3.3 T. Qualitatively the effect of decreasing magnetic induction is the same as decreasing stagnation temperature: a decrease of the maximum current accompanied by an increase of the inlet relaxation length. As a result of the variation of the relaxation length the electrical power of the generator is very strongly dependent on the magnetic induction. It is shown in Fig.6 that this dependence is stronger than quadratic. The analogy between the influence of the magnetic induction and of the stagnation temperature on the current behaviour suggests that at higher magnetic inductions power production may be realized at lower stagnation temperatures than 1700 K.

The maximum power obtained at an inlet stagnation temperature of 2000 K is 240 kW. In that case the enthalpy extraction is 11.5% (a reduction of 10 kW because of the power for the preionizer has been taken into account). The scattering in the points of Fig.6 is attributed to irregularities in the seed injection. An enthalpy extraction of 11.5% is considered as a maximum value which can be achieved at the given experimental conditions.

The long relaxation region obtained at low stagnation temperatures or low magnetic inductions cannot be described by one-dimensional calculations, because those calculations predict a steep increase of the current. Two-dimensional analyses yield relaxation lengths about equal to the height of the channel[6], whereas the experiments show a relaxation region which can be extended over several times the channel height, depending on the magnetic induction and the inlet stagnation temperature. Because in all the experiments the long relaxation lengths are accompanied by strong fluctuations measured in the radiation intensities as well as in the currents, it is believed that a proper description of the relaxation region has to include the characteristics of the discharge structure and the corresponding fluctuations of the quantities involved. Because of their essential role, discharge structure and fluctuation characteristics are studied in more detail.

IV. Discharge structure

The structure of the discharge has been investigated with an image converter camera. Streak pictures of the plasma in the core flow have been taken at different stagnation temperatures, magnetic inductions and load resistances. The conditions of the runs considered are listed in Table I. A typical streak picture is given in Fig.7. The total streak time is 140 μs and the projection of the length of the slit on the plasma is 2.0 cm. The figure shows an inhomogeneous discharge: a "streamer structure", as observed in Refs.1 and 2. All streamers apparently move with the same velocity, which is also constant during the streak time. Also the dimension of the streamers does not change during the time of observation. Fig.7 corresponds to a stagnation temperature of 3500 K. At stagnation temperatures of about 2000 K less streamers per streak time are observed, but they also have constant dimension and constant velocity. The streamer velocities, which immediately follow from the angle appearing on the streak picture, are compared with the gas velocity calculated from the gasdynamical program (Table I). It appears that the calculated gas velocity and the observed streamer velocity agree within about 10%. This is in agreement with the result of fluctuation analyses, where the same conclusion follows from the correlation between currents of different electrodes[3]. The fact that, even at high magnetic interaction (Lorentz force larger than pressure gradient), the streamers remain frozen in the gas flow demonstrates that there is a strong frictional interaction between the streamer and the gas flow.

Some streak observations were performed of the plasma close to the electrode wall at a distance of 6 mm. The observed streamer velocity is then no longer constant but has an irregular character. This behaviour can be explained by assuming that a streamer while moving with the gas flow changes its connection with the electrodes by jumping from one electrode to the next one (Compare Refs.7,8 and 9).

V. Fluctuation analysis

In this section a fluctuation analysis is applied to experiments at a stagnation temperature interval between 1840 and 2000 K. The model of Rosa[10] is used in which the non-uniformities have the form of parallel layers of high and low electrical conductivity. The model is shown in Fig.8. In this figure the gas flow u is in the x-direction and the magnetic induction B in the z-direction. A relation between the average of the current density and the electric field can be derived[10] for this model with $\phi = 0$:

$$\langle J_x \rangle = \rho \langle E_x \rangle - \langle \beta \rangle \rho \langle E^*_y \rangle$$

$$\langle J_y \rangle = \langle \beta \rangle \rho \langle E_x \rangle + \{ \langle \sigma \rangle - \langle \beta \rangle^2 \rho \} \langle E^*_y \rangle \qquad (1)$$

In eq.1 σ is the local conductivity, β the local Hall-parameter, $\rho = \langle \frac{1 + \beta^2}{\sigma} \rangle^{-1}$, and $\langle E^*_y \rangle = \langle E_y - uB \rangle$. The average $\langle\ \rangle$ is equal to $\frac{1}{S}\int ds$. Further we suppose the thickness of the layers with different plasma properties small compared to S and to the height of the channel. Boundary effects are not taken into account. For $\phi \neq 0$ Ohm's law can after a coordinate transformation be written as:

$$\langle J_x \rangle = \{\rho\cos^2\phi + \langle\sigma\rangle\sin^2\phi - \langle\beta\rangle^2\rho\sin^2\phi\} \langle E_x \rangle + \{\rho\sin\phi\cos\phi - \langle\beta\rangle\rho - \langle\sigma\rangle\sin\phi\cos\phi + \langle\beta\rangle^2\rho\sin\phi\cos\phi \} \langle E^*_y \rangle$$

$$\langle J_y \rangle = \{\rho\sin\phi\cos\phi + \langle\beta\rangle\rho - \langle\sigma\rangle \sin\phi\cos\phi + \langle\beta\rangle^2\rho\sin\phi\cos\phi \} \langle E_x \rangle + \{\rho\sin^2\phi + \langle\sigma\rangle\cos^2\phi - \langle\beta\rangle^2\rho\cos^2\phi \} \langle E^*_y \rangle \qquad (2)$$

Eq.2 now can be written in the simple two-dimensional form $\langle \bar{J} \rangle = \bar{\bar{\sigma}}_e \langle \bar{E}^* \rangle$. The elements of $\bar{\bar{\sigma}}_e$ are a function of ϕ and they are all different. Only for $\phi = 0$ the element $\sigma_{exy} = -\sigma_{eyx} = -\langle\beta\rangle\rho$.

Electron temperature and electron density and its fluctuations are measured by the recombination radiation at two wavelengths (4102 and 4897 Å) as described in Ref.3. The optical system was located at the 14th electrode pair. Fig.9 shows the recombination radiation at 4102 Å for several stagnation temperatures. It follows from the pictures that the relative fluctuation level is growing with decreasing stagnation temperature. The magnetic induction is nearly the same for all these runs. Run 1864 at 1830 K stagnation temperature and 2.85 T shows well pronounced regions of high and low intensities, which means high and low electron densities. These regions pass the optical system with a velocity about equal to the gas velocity. Apparently these regions are frozen in the gas flow. This conclusion is supported by strong correlation between the radiation and nearest electrode current. This correlation is illustrated in Fig.10. Because the non-uniformities are frozen in the gas flow time averages and space averages in the x-direction are equal. Given the velocity of the gas (about 1000 m/s) the thickness of the non-uniformities is around 1 cm (Fig.9f).

From the radiation measurements a probability density function is found for the electron density n_e. Using the local expressions

$$\sigma = \frac{e^2 n_e}{m_e \nu(n_e)} \quad \text{and} \quad \beta = \frac{eB}{m_e \nu(n_e)} \qquad (3)$$

the tensor elements of $\bar{\bar{\sigma}}_e$ can be calculated for each run. The elements are still a function of ϕ. In Eq.3 Coulomb collisions are taken in account. Table II shows the values for $\langle\sigma\rangle$, $\langle\beta\rangle$, σ_{exx}, σ_{exy} and σ_{eyy} for $\phi = 0$ for a number of runs. Further it shows the average fields $\langle E_x \rangle$ and $\langle E^*_y \rangle$ measured by probes in the wall of the generator channel. The values of uB are taken from the gasdynamical program. The last four colums contain the calculated values $\langle J_x \rangle$, $\langle J_y \rangle$ and $\langle J \rangle = \sqrt{\langle J_x \rangle^2 + \langle J_y \rangle^2}$ using Eq.2. Further J_{14}, the measured current density at the 14th electrode pair, which is near the optical system, is given. If it is assumed that the total current in the bulk of the plasma flows into the electrodes, it can be concluded from the table that there is a good agreement between the calculated $\langle J \rangle$ and the measured J_{14}.

The next step in our analysis is to investigate how the calculated current densities $\langle J_x \rangle$ and $\langle J_y \rangle$ depend on the angle ϕ of the streamers. Using the radiation measurements we calculate $\langle J_x \rangle$, $\langle J_y \rangle$ and $\langle J \rangle$ from Eq.2 as a function of ϕ. It follows that $\langle J \rangle$ and $\langle J_x \rangle / \langle J_y \rangle$ are only weak functions of ϕ. Since the direction of the inhomogenities is not strongly related to the current density we may use the two-dimensional theory of M.Martinez-Sanchez[11]. This theory is based on a certain class of unbounded plasmas with isotropic inhomogenities. In this case the two-dimensional effective Ohm's law reads as follows:

$$\begin{bmatrix} \langle J_x \rangle \\ \langle J_y \rangle \end{bmatrix} = \frac{\sigma}{1 + \beta_e^2} \begin{bmatrix} 1 & -\beta_e \\ \beta_e & 1 \end{bmatrix} \begin{bmatrix} \langle E_x \rangle \\ \langle E^*_y \rangle \end{bmatrix} \qquad (4)$$

with

$$\frac{\sigma_e}{\langle\sigma\rangle} = \frac{\beta_e}{\langle\beta\rangle} = 1 \Big/ \sqrt{\langle \frac{1 + \beta^2}{\sigma} \rangle \langle\sigma\rangle - \langle\beta\rangle^2} \qquad (5)$$

The same procedure as described in Ref.3 is used to calculate σ_e and β_e. Then $\langle J_x \rangle$ and $\langle J_y \rangle$ can be found using the measured fields $\langle E_x \rangle$ and $\langle E^*_y \rangle$ and Eq.4. The results are shown in Table III. Again there is a good agreement between the calculated current density $\langle J \rangle$ and the measured one at electrode pair 14.

The energy equation for electrons in its simplest form is as follows

$$\langle \bar{J} \rangle . \langle \bar{E}^* \rangle = 3 \langle n_e \rangle k (\langle T_e \rangle - T_g) * \left(\langle \nu_{ei} \rangle \frac{m_e}{m_s} + \langle \nu_{eh} \rangle \frac{m_e}{m_h} \right) \quad (6)$$

in which the left hand side is the Ohmic heating and the right hand side the elastic loss term. ν_{ei} is the collisions frequency between electrons and cesium ions, ν_{eh} the collision frequency between electrons and argon atoms. m_e is the electron mass, m_s the mass of a cesium atom and m_h of an argon atom. The right hand side of Eq.6 can be calculated using the measured average values of n_e and T_e. The left hand side can be calculated for three different situations:

a. using the model with vertical streamers ($\phi = 0$),
b. using the model with $\phi = \arctan(-\langle J_x \rangle / \langle J_y \rangle)$ which means that the average current density has the same direction as the streamer, and
c. using M.Martinez-Sanchez[11] model for isotropic inhomogenities. The results of the calculations are collected in Table IV. The table shows that at these low stagnation temperatures agreement can be obtained for two models: the isotropic model or the model with a well defined angle ϕ with $0 < \phi < \arctan(-\langle J_x \rangle / \langle J_y \rangle)$.

Conclusions

The generator performance has been investigated for inlet stagnation temperatures equal and below 2000 K. No power production was measured at stagnation temperatures lower than 1700 K. The decrease of the electrical power is caused by a strong increase of the inlet relaxation length in combination with a gradual decrease of the maximum current. The stagnation temperature of 1700 K should not be considered as an absolute minimum, for power production, especially because of the observed influence of the magnetic indcution. It is expected that the medium will still be sufficiently electrically conductive at stagnation temperatures belowe 1700 K if magnetic inductions larger than 3 T are applied. At an inlet stagnation temperature of 2000 K a maximum enthalpy extraction of 11.5% has been achieved.

It follows from fast photography observations that the discharge has an inhomogeneous structure under all experimental conditions considered. The streamer structure is more pronounced at low stagnation temperatures. The streamers move through the generator frozen in the bulk of the gas, also in cases when the Lorentz force is larger than the pressure gradient, which demonstrates a large frictional interaction between the streamers and the gas flow. Close to the electrode wall the streamer velocity is irregular and no longer equal to the gas velocity, which may be explained by changes in the connections between streamers and electrodes.

Going down in stagnation temperature (from 3500 to 2000 K) the relative fluctuation level in electrode current as well as in electron density becomes higher. There is no significant change in electron temperature fluctuation level, it remains 10%. A strong correlation is observed between electrode currents and the radiation at the same position in the generator channel. The model with nonuniformities in the form of parallel layers predicts current densities which are close to the measured ones. The total current density and its direction is nearly independant of the chosen streamer angle. The theory based on isotropic inhomogenities in the plane perpendicular to the magnetic field predicts current densities which are also in agreement with the measured ones.

Acknowledgement

This work was performed as a part of the research program of the Group Direct Energy Conversion of the Eindhoven University of Technology. The authors wish to express their thanks to G.van Brussel, A.van Iersel, H.F.Koolmees, A.F.C. Sens and J.P.Verhagen for their contribution to the development of the diagnostics and the data handling, and their assistance in operating the facility.

References

1. Zauderer, B., Phys.Fluids 11, p.2577, 1968.
2. Brederlow, G., et al., AIAA J., 11, p.1065, 1973.
3. Hellebrekers, W.M., et al., Proc.16th Symp. Eng. Asp. of MHD, II.3.14, Pittsburgh, 1977.
4. Veefkind A., et al., AIAA J.14, p.1118, 1976.
5. Blom J.H., et al., Proc.15th Symp.Eng.Asp. of MHD, VI.5, Philadelphia, 1976.
6. Blom, J.H. and Houben, J.W.M.A., Proc.5th Int. Conf.on MHD Power Generation, II, p.65, 1971.
7. Baranov, V.Yu. and Vasil'eva, I.A., High Temperature 2, p.609, 1964.
8. Baranov, V.Yu. and Vasil'eva, I.A., High Temperature 3, p.155, 1965.
9. Baranov, V.Yu., High Temperature 4, p.585, 1966.
10. Rosa, R.J., Phys.Fluids 5, p.1081, 1962.
11. Martinez-Sanchez, M.et al., Proc.6th Int.Conf. on MHD Electric Power Generation, IV.247, Washington D.C., 1975.

Table I. Runs for discharge observations.

Stagn. temp. (K)	Magnetic induction (T)	Load resistance (Ω)	Gas velocity (m/s)	Streamer velocity (m/s)
3660	3.15	2.26	1100	1150
3680	3.09	2.26	1110	1220
3870	2.76	2.26	1210	1250
3710	2.46	2.26	1270	1350
3760	2.02	2.26	1320	1340
3750	1.53	2.26	1450	1470
3680	1.24	2.26	1480	1470
1990	3.22	1.26	780	870
2000	2.42	1.26	990	1060
1990	1.95	1.26	1100	1050
1960	3.20	1.26	990	1080
2030	3.12	1.26	950	1100
2050	3.04	1.26	1010	980
2010	2.24	1.26	970	1130
2000	2.76	1.26	1090	1040
1970	2.44	1.26	1080	1040
2000	2.41	1.26	1090	1140

Table II. Comparison between calculated and measured current densities using the layer model.

Run	B T	T_s K	T_g K	$<\sigma>$ mho/m	$<\beta>$	σ_{exx} mho/m	σ_{exy} mho/m	σ_{eyy} mho/m	$<E_x>$ V/m	$<E_y>$ V/m	$<J_x>$ kA/m^2	$<J_y>$ kA/m^2	$<J>$ kA/m^2	J_{14} kA/m^2
1967	3.16	1970	1150	217	12.0	1.5	-17.4	8.3	-1100	-1740	29	- 34	45	46
1969	3.03	2000	1210	246	10.1	2.3	-23.6	8.4	-1150	-1440	31	- 39	50	49
1971	3.38	1970	1230	229	12.3	1.5	-18.2	6.0	-1230	-2020	35	- 35	49	42
1973	3.16	2010	1090	215	10.9	1.7	-18.8	9.5	-1310	-1760	31	- 41	52	47
1974	3.12	1990	1100	223	10.4	2.0	-20.8	6.7	-1240	-1530	29	- 36	46	46

Table III. Comparison between calculated and measured current densities using model of isotropic inhomogenities.

Run	σ_e mho/m	β_e	$<J_x>$ kA/m^2	$<J_y>$ kA/m^2	$<J>$ kA/m^2	J_{14} kA/m^2
1967	88	4.9	27	- 31	41	46
1969	129	5.3	28	- 32	42	49
1971	114	6.1	33	- 28	44	42
1973	91	4.7	29	- 34	44	47
1974	121	5.7	26	- 25	37	46

Table IV. Electron energy balance check for three mentioned cases.

Run	Coll.losses Mw/m^3	Ohmic heating a	b	c
1967	13.3	28.4	6.8	15.1
1969	16.0	20.5	8.2	15.1
1971	14.3	26.7	8.2	16.7
1973	17.9	32.4	8.6	19.5
1974	17.8	18.8	7.7	14.2

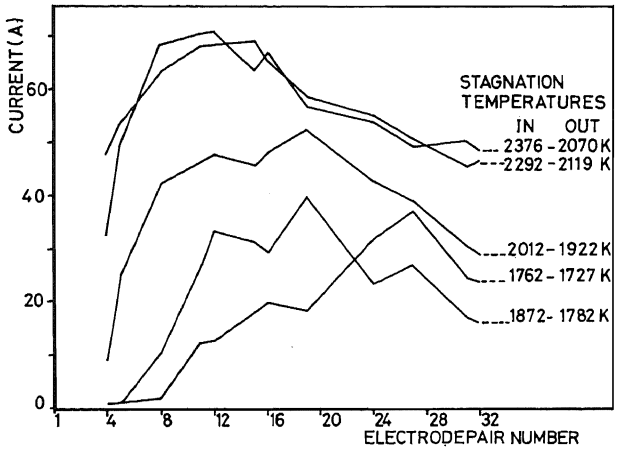

Figure 1. Current along the generator at various stagnation temperatures. B = 3 T. R_{load} = 2.26 Ω.

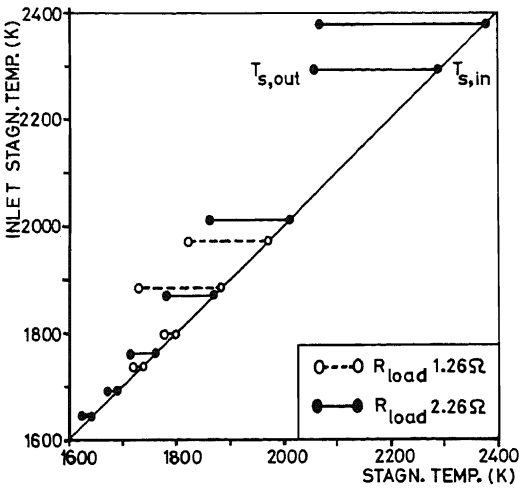

Figure 2. Stagnation temperature ranges.

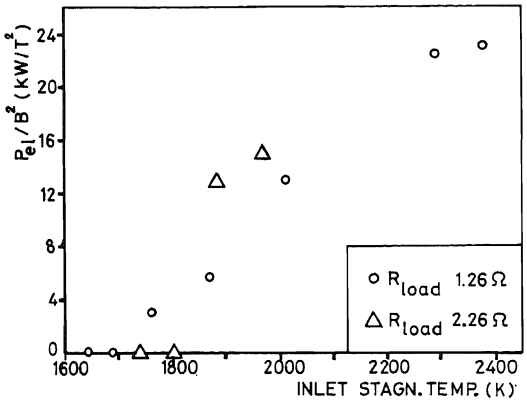

Figure 3. Electrical power at various inlet stagnation temperatures. B = 3 T.

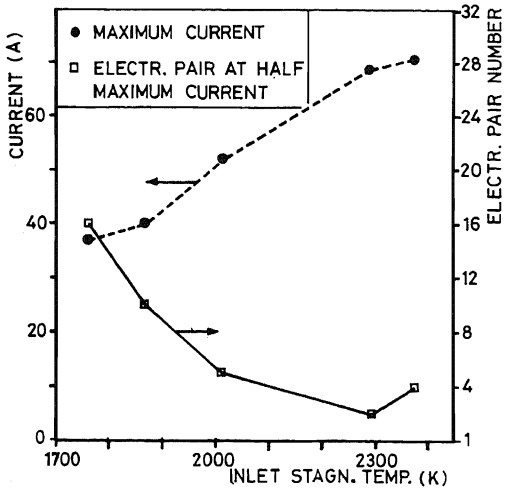

Figure 4. Influence of the inlet stagnation temperature on the current level and the relaxation length. B = 3 T. R_{load} = 2.26 Ω.

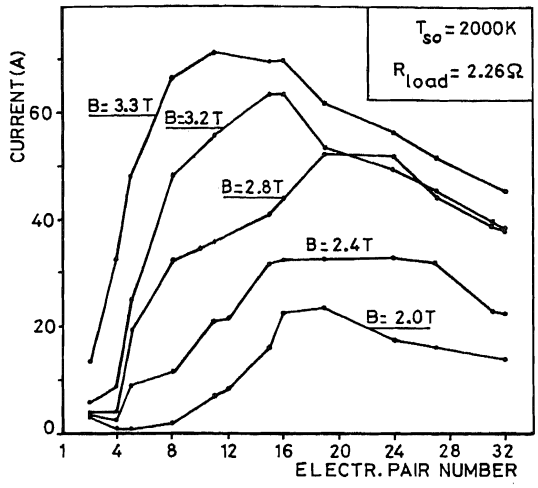

Figure 5. Current along the generator at various magnetic inductions.

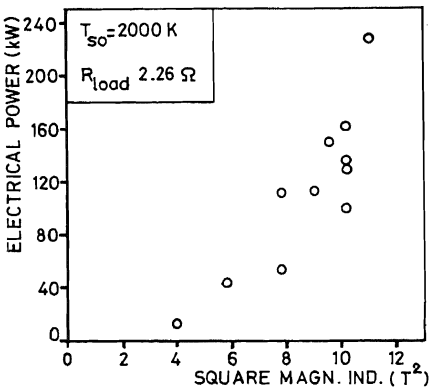

Figure 6. Influence of the magnetic induction on the electrical power.

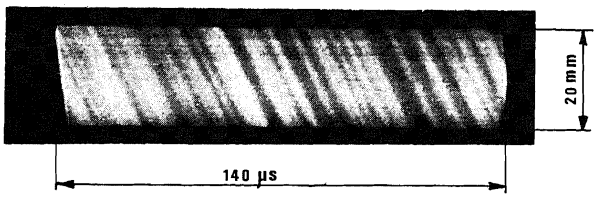

Figure 7. Streak picture.

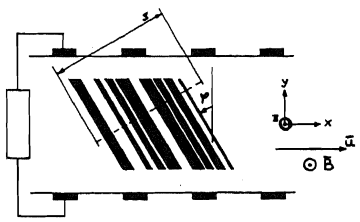

Figure 8. Model for streamer nonuniformities in an MHD generator. The streamers have an arbitrary angle ϕ with y-direction.

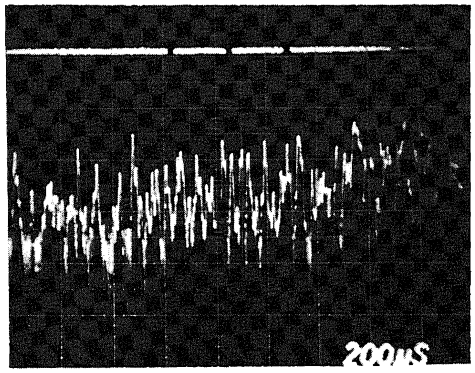

Figure 9a. Run 1859: B = 2.84 T, T_s = 3750 K, T_g = 2420 K, I_{14} = 99.5 A.

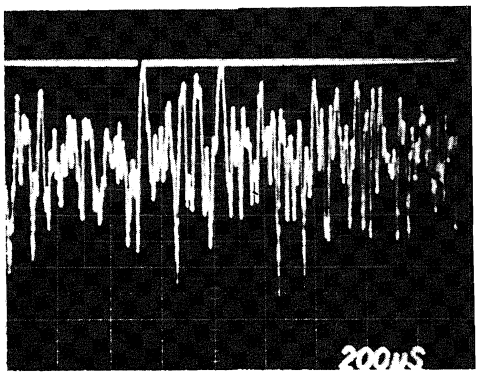

Figure 9b. Run 1863: B = 2.64 T, T_s = 2240, T_g = 1050 K, I_{14} = 88.3 A.

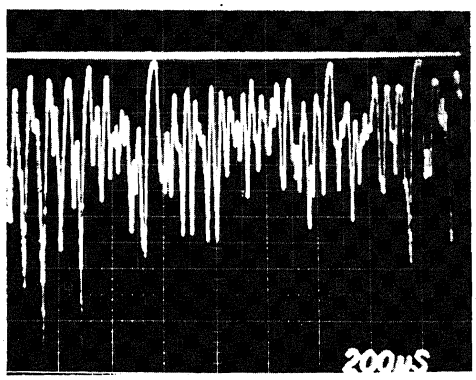

Figure 9c. Run 1865: B = 2.85 T, T_s = 2090 K, T_g = 1120 K, I_{14} = 79.4 A.

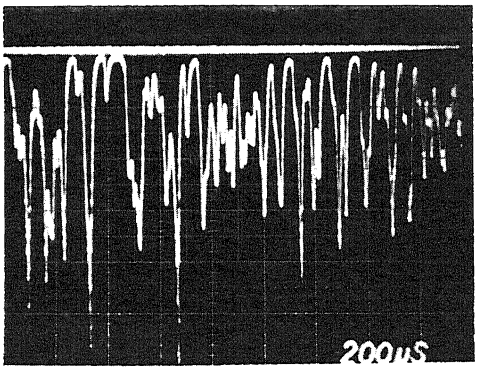

Figure 9d. Run 1866: B = 2.74 T, T_s = 2000 K, T_g = 900 K, I_{14} = 61.9 A.

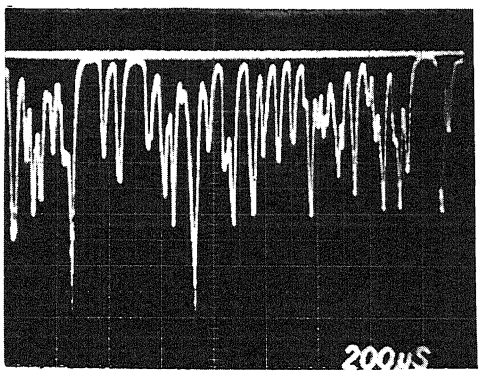

Figure 9e. Run 1875: B = 3.17 T, T_s = 1900 K, T_g = 880 K, I_{14} = 68.6 A.

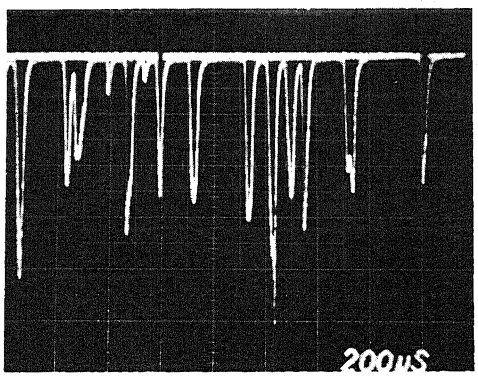

Figure 9f. Run 1864: B = 2.85 T, T_s = 1840 K, T_g = 810 K, I_{14} = 34.3 A.

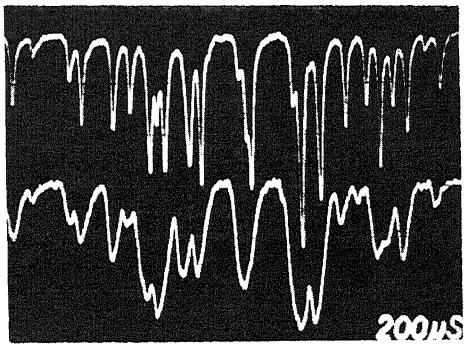

Figure 10. Correlation between radiation at 4102 Å (upper trace) and the electrode current (lower trace).